Climatic Change (2015) 129:511–523
DOI 10.1007/s10584-013-0885-2

Long-term simulation of large-scale urbanization effect on the East Asian monsoon

Jin-Ming Feng · Yong-Li Wang · Zhu-Guo Ma

Received: 31 January 2013 / Accepted: 18 August 2013 / Published online: 13 September 2013

Abstract The Weather Research and Forecasting (WRF) model is used to simulate the long-term effect of urbanization on regional climate, especially the East Asian monsoon. Besides land use change from urbanization, anthropogenic heat release is an important factor for the urban climate and environment, so these two factors are included in the simulation. Two experiments were designed and executed for the 10-year period. Urbanization is not considered in one experiment, and in the other, urban land use and anthropogenic heat release are comprehensively investigated. Comparison of the two runs shows that urbanization mainly decreases low-cloud cover across most of East China, and nearly all surface energy fluxes increase except those of latent heat and upward shortwave. Based on a multiyear average, the urbanization reduced summer precipitation in urban agglomerations, but the interannual variability is very large. Local upwelling airflow is strengthened by urbanization; however, additional precipitation was not produced because of a decline of surface moisture in urban agglomeration areas. From 850 hPa circulation change and the East Asian monsoon index, the summer monsoon is strengthened slightly and the winter monsoon is always weakened by large-scale urbanization.

1 Introduction

Evidence of impacts of anthropogenic climate change in all aspects of the natural world and on human activity is steadily increasing, and has become an issue of pressing political and social concern. The Intergovernmental Panel on Climate Change (IPCC 2007) noted that global temperature increased 0.74 °C over the past 100 years. This indicates that greenhouse gas emissions are the main cause of global warming and that climate effects of urbanization may be negligible on the global scale. However, the expansion of urban areas has caused a series of changes, including increases of sensible heat flux and urban temperature, decreases of evaporation, and even time-specific variations of regional atmospheric stratification stability (Jiang et al. 2009). Therefore, while climate effects of urbanization may be

This article is part of a Special Issue on “Regional Earth System Modeling” edited by Zong-Liang Yang and Congbin Fu.

J.-M. Feng (✉) · Y.-L. Wang · Z.-G. Ma
Key Laboratory of Regional Climate-Environment for East Asia, Institute of Atmospheric Physics, Chinese Academy of Sciences, Beijing 100029, China
e-mail: fengjm@tea.ac.cn

negligible on the global scale, regional and local effects of urbanization cannot always be neglected.

With the rapid development of cities, there has been growing interest in studying the urban heat island (UHI). Urban warming and its impact on regional and local climate have been well documented in several mature cities in Europe, North America and Asia, including Beijing and cities in Japan, the Yangtze River Delta region, and Taiwan. Emmanuel and Krüger (2012) found that within the period around 1985–1995, minimum temperatures in Glasgow maintained warmer values than in regional trends. Jones et al. (2008) used sea surface temperature (SST) datasets to assess potential urban influences on the East China mainland. They showed that urban-related warming across China was approximately 0.1 °C per decade during 1951–2004, with overall climatic warming at 0.81 °C.

In addition to this land use change from urbanization, it is likely that anthropogenic heat sources will be important in reaching an urban surface energy balance in the future (Allen et al. 2010). Anthropogenic heat flux varies spatially and temporally and, under certain conditions, can exceed energy receipt from net all-wave radiation (Lee et al. 2009). A comparison between absorbed shortwave solar radiation and anthropogenic heat emissions of London buildings indicated that total heat emission from buildings during a winter day was between 3 and 25 times greater than incident solar radiation; during a summer day it was between 0.04 and 0.4 times, depending on built form density (Hamilton et al. 2009). Zhang et al. (2013) used a heat balance model and satellite images from 1989 to 2001 together with meteorological station data to study the urban thermal environment in the city of Fuzhou, China. The results suggest that anthropogenic heat release is likely significant in the UHI effect, and must be considered in urban climate change adaptation strategies.

At present, UHI intensity is often estimated by using the difference between urban and rural temperatures from individual observing locations. Some researchers have used numerical models to study the impact of urbanization on climate change at global and regional scales, and even in large individual cities. However, there are few simulation studies of long-term effects of urbanization on climate at regional scale. One example was statistically significant continental-scale surface warming (0.4 –0.9 °C) in one 2100 anthropogenic heat release (AHR) scenario, simulated by a general circulation model (GCM) using future AHR global inventories (Flanner 2009). Zhang et al. (2010) suggested that mean surface air temperature in urbanized areas increased in winter and summer across the Yangtze River Delta. Lin et al. (2011) found that the UHI effect significantly perturbs thermal and dynamic processes. Shem and Shepherd (2009) found increased rainfall downwind of Atlanta, via Weather Research and Forecasting (WRF) model simulation. Zhang et al. (2009) indicated that effects of expanding urban surfaces are responsible for reducing precipitation over the Beijing area during summer and winter.

Feng et al. (2012) used the WRF/Urban Canopy Model (UCM) to simulate regional climate impacts of urbanization and anthropogenic heat release in China. Their period of integration was only 2 years (2007–2008), and AHR processing was relatively simplistic. Only three values of annual-mean AHR were assigned to urban types (industrial/commercial, high and low-density residential), and the annual AHR cycle was not included. Wang et al. (2012) performed nested, high-resolution modeling of three vast urban agglomerations in China, but only focused on effects of urban land use change, with a simulation period of only three years. Because of such short periods and simplified designs, there are likely substantial uncertainties in the aforementioned simulation results.

In this work, WRF was used to simulate the long-term effect of urbanization on regional climate, especially the East Asian monsoon. A more reasonable parameterization of AHR was evaluated, and a more appropriate configuration of physical schemes was used for long-term simulation.

2 Model details and experimental design

Simulation was done using of WRF version 3.3 with the Advanced Research WRF (ARW) dynamic core (Skamarock et al. 2008). The Noah land surface model (Chen and Dudhia 2001) with UCM (Chen et al. 2010) was also used. Forcing fields, such as large-scale atmospheric fields, sea surface temperature (SST) and initial soil parameters, including soil moisture and temperature, were from the 1°×1° NCEP Global Final Analysis (FNL) 6-hour data (Research Data Archive at the National Center for Atmospheric Research et al. 1999; http://rda.ucar.edu/datasets/ds083.2/). The model domain (Fig. 1a) has a horizontal resolution of 30 km. The simulation period was from 1 January 2000 to 28 February 2010. Deep soil temperature was updated during the simulations.

Two experiments were designed and carried out. In the control run (Ctr), International Geosphere Biosphere Programme—Moderate Resolution Imaging Spectroradiometer (IGBP-MODIS) 20-category (Friedl et al. 2002) land-use data were used, and urban type was replaced by vegetation type of the nearest-neighbor grid. In the sensitivity run (Sen), MODIS 33-category data (Chen et al. 2010), including three urban categories, were used, and gridded AHR was added to the corresponding urban grid. Based on population and the energy use, urban area was divided into three types: industrial/commercial, and high-and low-density residential. Except for AHR values, we used the default urban parameters for these three urban types of WRF/UCM. Table 1 in Wang et al. (2012) shows the urban parameters of high-density residential type. Based on the China City Statistical Yearbook (2009a) and China Energy Statistical Yearbook (2009b), urban land-use and AHR data were constructed. However, not all of the urban has the energy use data. Therefore, for grids where the land-use type is urban but the AHR is missing, the average AHR of all the other urban grids with AHR values is adopted. The spatial distribution of AHR in China is shown in Fig. 1b.

In WRF/UCM, each urban type can only have one AHR value, and AHR has a prescribed diurnal change for three urban categories, without a seasonal cycle. In fact, AHR has a seasonal cycle and spatial distribution in the real world. Because of the lack of seasonal energy-consumption data, the AHR seasonal cycle is parameterized in the simulation (Flanner 2009). In this approach, the seasonal weighting function depends on fractional time of year (t_y). The higher the latitude, the greater the amplitude of the seasonal cycle, and this cycle is not applied to regions equatorward of 33°. The AHR magnitude in winter is larger than that in summer. The detailed formula is

$$\mathrm{W_y}\left(\mathrm{t_y}\right) = 1 + \mathrm{A_2}(\theta)\sin\left[2\pi\left(\mathrm{t_y} + 0.25\right)\right], \textit{where } \theta \textit{ is latitude in degrees}.$$

The latitudinally-dependent amplitude is

$$\begin{aligned} \mathrm{A_2}(\theta) &= 1 - e^{(-\theta-33)/25} && \textit{for } \theta > 33 \\ \mathrm{A_2}(\theta) &= 1 && \textit{for} -33 \le \theta \le 33 \\ \mathrm{A_2}(\theta) &= -\left(1 - e^{(\theta+33)/25}\right) && \textit{for } \theta < -33 \end{aligned}$$

The above AHR parameterization was introduced into the model. As in the original version, AHR was added to the calculation of surface energy budget as sensible heat. However, through the adjustment of surface energy fluxes, the net radiation and the AHR can be re-partitioned to sensible heat and latent heat.

The Beijing–Tianjin–Hebei, the Yangtze River Delta and the Pearl River Delta regions are the most important urban agglomerations in China. Since the mid-1980s, mass labor

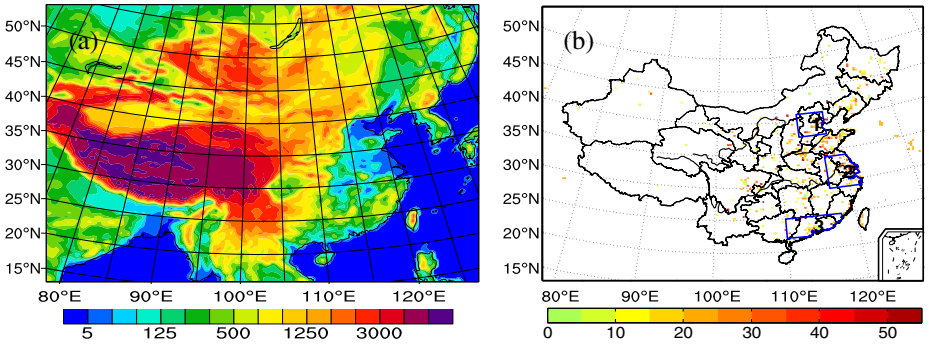

Fig. 1 **a** Model domain and elevations (m). **b** Spatial distribution of anthropogenic heat flux (W/m^2) and regional divisions (1, Beijing–Tianjin–Hebei region; 2, Yangtze River Delta region; and 3, Pearl River Delta region)

migration from the countryside to urban areas has been one of the most dramatic and noticeable changes in the country, particularly in those agglomerations. These have also had the greatest increases in urban development nationwide. Some other regions may have had significant increases, but areal extents of these were smaller. Thus, the following analyses mainly focus on the three sub-regions (Fig. 1b).

3 Results

3.1 Comparison between simulation and observation

Relevant research has demonstrated that the WRF model performs well in simulating the mean climate of China (Feng et al. 2012). Here, we compare the observed and WRF-simulated annual average 2-m air temperature and precipitation. Climatological mean monthly surface air temperature data are from 740 stations in China (Zhao and Fu 2006) and precipitation is based on Tropical Rainfall Measuring Mission (TRMM) data (Huffman et al. 2007).

The simulation results indicate that the spatial distribution of model temperature is basically consistent with observation, with a low-temperature area in the Yangtze River Delta. The observed precipitation pattern is characterized by less precipitation in North China and more precipitation in the south. Overall, model precipitation captures the patterns and magnitudes well over most of the country. Precipitation in the south is overestimated (not shown).

The 10-year simulation permits comparison of its interannual variation and that of observation. Anomalies of observed and simulated annual average temperatures across China and the three sub-regions during 2000–2009 are shown in Fig. 2. The correlation

Table 1 Temporal correlation coefficients between control run and observation across different regions

	China	Beijing-Tianjin-Hebei	Yangtze River Delta	Pearl River Delta
Temperature	0.84	0.75	0.82	0.89
Precipitation	0.65	0.36	0.45	0.57

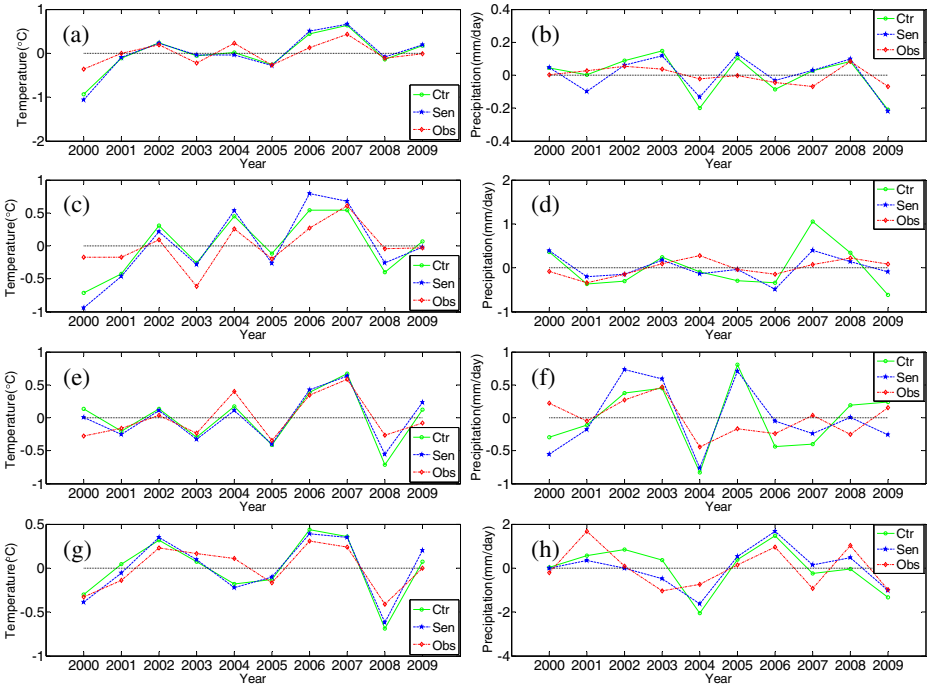

Fig. 2 Interannual variation of anomalies of observed and simulated annual average temperatures (*left*: °C) and precipitation (*right*: mm/day) across different regions during 2000–2009. **a**, **b**: China; **c**, **d**: Beijing–Tianjin–Hebei; **e**, **f**: Yangtze River Delta and **g**, **h**: Pearl River Delta

coefficients of yearly temperature and precipitation between the simulation and observation are shown in Table 1.

Across the entire country on average, the reproduced interannual temperature variation is consistent with the observation, except for small deviations in 2000 and 2006. The correlation coefficient of yearly temperature in the country between simulation and observation is 0.84. Among the three urban agglomerations, the Beijing–Tianjin–Hebei region has a relatively large simulation bias. In the Yangtze and Pearl River Deltas, the simulation basically agreed with observation, except for 2004 and 2008. The simulated temperature in the Pearl River Delta has a high correlation coefficient of 0.89 with observation.

In comparison with observational data, simulated precipitation fluctuations are large. Considering all of China, the absolute value of the simulated precipitation anomaly is less than 0.2 mm/day, and the correlation coefficient is 0.65 between simulation and observation. The Yangtze and Pearl River Delta regions have similar changes, but with relatively large fluctuations. Correlation coefficients between simulated and observed precipitation are 0.36, 0.45, and 0.57 in the three urban agglomerations, respectively.

Compared with temperature, simulation of interannual precipitation variation is very difficult, especially in the East Asian monsoon region. Bias has two main sources; one is the large-scale forcing field, and the other is the complexity of physical processes in the regional model. In light of the comparison between simulation and observation, the WRF model can show the major characteristics of multiyear regional and East Asian monsoon climate.

3.2 Changes of temperature and precipitation from urbanization

Temperature and water conditions on the Earth's surface, including surface air temperature, precipitation, soil temperature and moisture, are closely related to human life. Urbanization can clearly affect temperature and moisture on regional and local scales.

Figure 3 shows monthly surface air temperature and precipitation change due to urbanization as 10-year averages over each region. Error bars represent the 95 % confidence interval of estimated 10-year average change. They also indicate the relative magnitude of interannual variability of 10-year temperature and precipitation change caused by urbanization. The magenta diamonds show that the difference of the simulated results between Sen run and Ctr run is statistically significant at alpha=0.05, i.e. exceed 95 % confidence level. Over the entire country, maximum temperature change is in August, and interannual variability is large from July through September. Only the temperature change in June exceeds the 95 % confidence level. In the Beijing–Tianjin–Hebei region, the peak temperature change and its maximum interannual variability are in August and the changes are statistically significant from May through September except June. In the Yangtze River Delta, temperature change from May through September is large. The changes from March to October exceed the 95 % confidence level, but interannual variability in February is the greatest. However, there is no apparent difference between winter and summer in the Pearl River Delta with the changes from April through September exceeding the 95 % confidence level. The seasonal difference of temperature change due to urbanization is larger in high

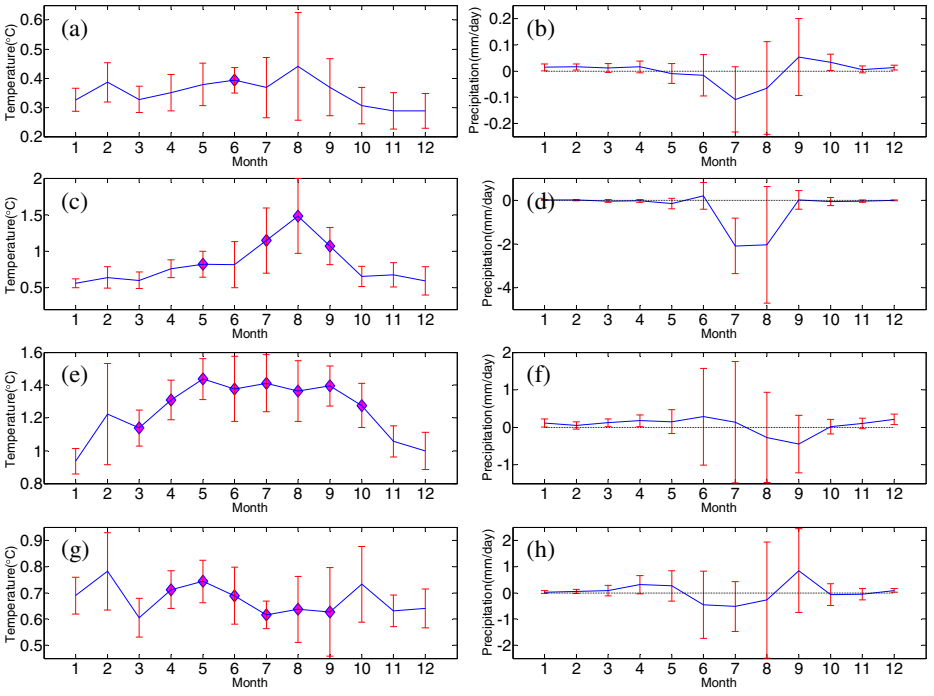

Fig. 3 Monthly temperature (*left*: °C) and precipitation (*right*: mm/day) change as ten-year averages across each region caused by urbanization. Error bars represent the 95 % confidence interval of estimated 10-year average change. Magenta diamonds denote the months through significance test at alpha=0.05. **a**, **b**: China; **c**, **d**: Beijing–Tianjin–Hebei region; **e**, **f**: Yangtze River Delta region; **g**, **h**: Pearl River Delta region

latitude areas than that in the low latitude. On one hand, the higher the latitude, the larger the seasonal cycle of regional climate, especially water vapor condition which is the most important factor for urbanization resulting in urban heat island, and the larger the seasonal difference of temperature change due to the urban underlying surface change. On the other hand, the ratio of AHR and incident solar radiation in winter is larger than that in summer, but the lower the latitude, the smaller the seasonal difference of this ratio.

From the figure of precipitation change, the confidence intervals and the interannual variabilities are very large from June to September. Across all China and the Beijing–Tianjin–Hebei region there is reduced precipitation from urbanization in July and August, and the interannual variability in August is very large. This indicates that the amplitude of August precipitation change greatly varies, and precipitation in this month does increase in certain years. In the Yangtze River Delta, precipitation increases except in August and September. In the Pearl River Delta, precipitation decreases from June to August and increases in most other months, especially during spring and September. The interannual variability is large in the Yangtze and Pearl River Delta from June through September. In all sub-regions, August precipitation change from urbanization has a large interannual variability. There is no change exceeding the 95 % confidence level in the regions.

3.3 Low cloud cover and surface energy budget

Clouds affect temperature by reflecting solar shortwave radiation and enhancing downward longwave radiation. Low cloud is important in the surface energy balance. However the output of WRF includes a 3-dimensional cloud cover on every sigma layer, and low cloud cover is not a variable in WRF. Referring to the definition of low cloud cover in ERA-Interim, the fractions of cloud cover on the layer with sigma >0.8 are used to calculate the low cloud cover. The maximum fractional cloud cover on these layers is defined as the low cloud cover. Observed low-cloud cover is from European Centre for Medium-Range Weather Forecasts Reanalysis (ECWMF) Interim (ERA-Interim) data (Dee et al. 2011). From the spatial distribution of low cloud cover in ERA-Interim data (Fig. 4a and d), low cloud cover is slight in North China, but substantial in the south, especially in Sichuan and

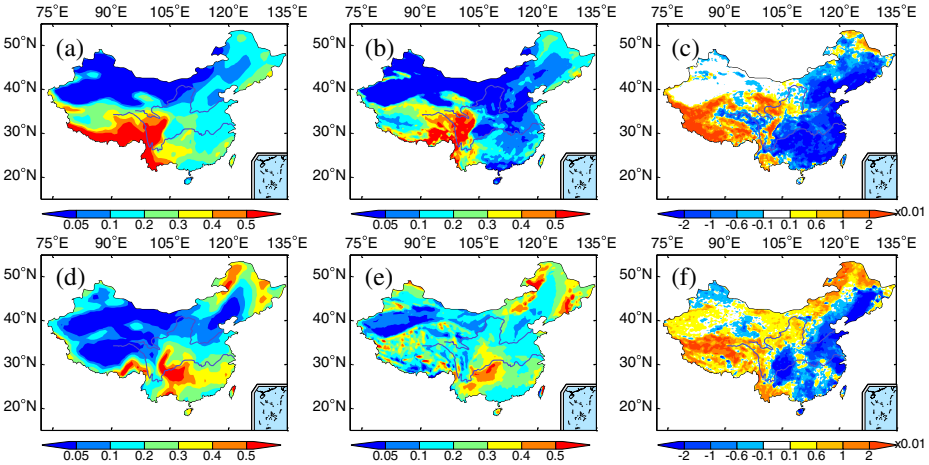

Fig. 4 Comparison and change of low cloud cover in summer (*top*, Unit: fraction) and winter (*bottom*, Unit: fraction); **a**, **d**: ERA-Interim; **b**, **e**: Ctr; **c**, **f**: Sen-Ctr

Yunnan provinces. In contrast to summer, winter has greater cover. The model can reproduce the basic pattern of low cloud cover, but compared with ERA-Interim data, the simulation is underestimated in summer in most areas (Fig. 4b and e). From the change of low cloud cover (Fig. 4c and f), urbanization reduced summer and winter low cloud cover over most of East China, where most cities are located. However, in West China, with fewer cities, there was increased cover, which may be caused by perturbation of atmospheric circulations.

The reduced low cloud cover increases incident solar shortwave radiation at the surface, enhancing urban warming. The increase of incident solar radiation can be seen in Fig. 5. The balance of energy and radiation is vital in the climate system. Urbanization mainly acts to change the surface energy balance to influence regional and local climates and environment. Figure 5 shows the changes of annual regional average surface energy fluxes caused by urbanization. Error bars represent the 95 % confidence interval of estimated 10-year average flux change. Surface latent heat flux and upwelling shortwave radiation decrease, and almost all other energy fluxes increase. With urbanization, city buildings trap more solar radiation because of multiple reflections, absorbed solar radiation increases and surface albedo declines. Because the surface changes from that of a nonurban area to a waterproof one mostly made of cement, available moisture decreases greatly and latent heat flux diminishes. Meanwhile, AHR is added to the surface as sensible heat. With such a sensible heat increase, surface temperature increases and other energy components adjust correspondingly, to reach a new energy balance. With the increased temperature, upward and downward longwave radiation increase. Although a decrease in low warmer clouds would decreases downward longwave radiation, but the simulated downward longwave radiation increases, this should be caused by the increase of lower atmospheric temperatures. Compared to the temperature and precipitation, the confidence intervals of the flux changes are small, and it also means the interannual variabilities are small. The interannual variability of surface downward solar radiation change is relatively larger than the other surface flux changes.

3.4 Circulation and East Asian monsoon index

In metropolitan areas, the urban canopy increases surface roughness, which strengthens vertical dynamic and thermal turbulence exchange while reducing wind speed. Urban warming intensifies vertical motion and convective activity, and generates local circulations. Therefore, large-scale urbanization may affect regional circulations to some extent.

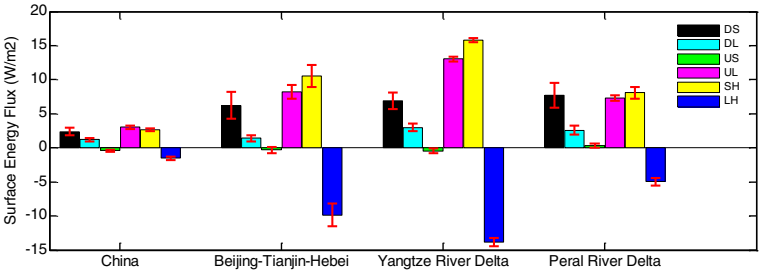

Fig. 5 The change of the annual regional average surface energy fluxes caused by urbanization (W/m^2). Error bars represent the 95 % confidence interval of estimated 10-year average flux change. DS: downward shortwave, DL: downward longwave, US: upward shortwave, UL: upward longwave, SH: sensible heat, LH: latent heat

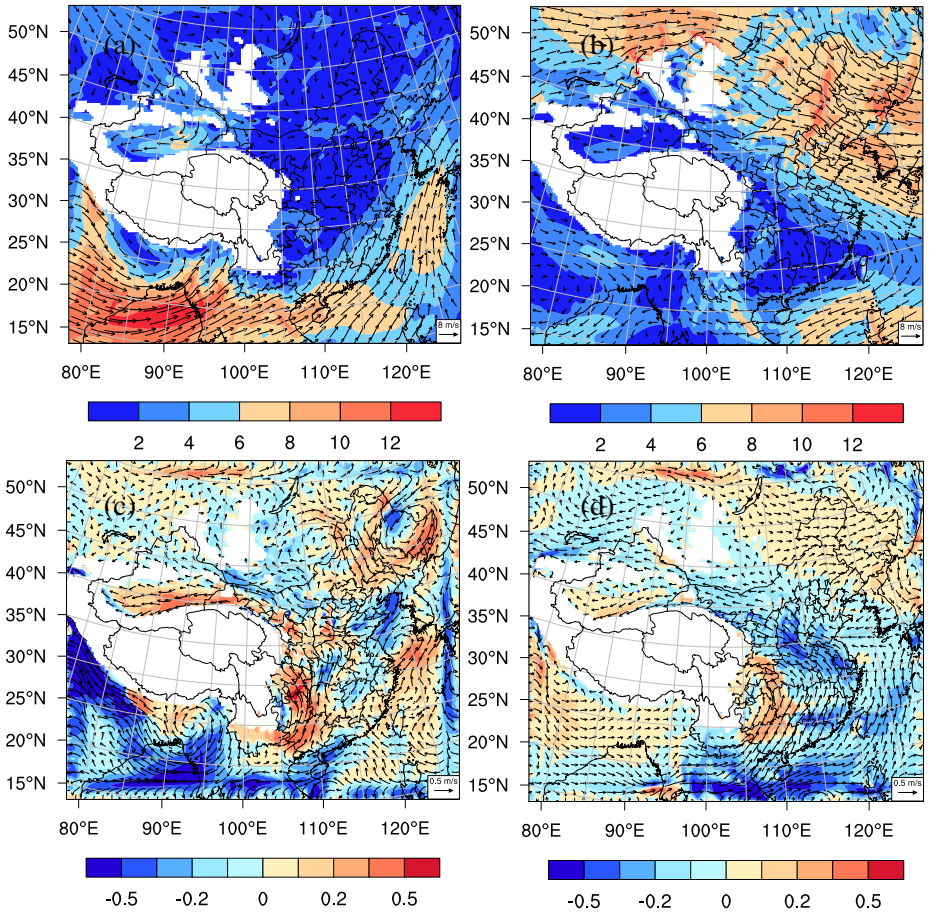

Fig. 6 850 hPa circulation of control run in summer (**a**) and winter (**b**), plus its summer (**c**) and winter (**d**) change caused by urbanization. Shading represents wind speed and its change (Unit: m/s)

Asian summer monsoon circulations, characterized by upper-air northeasterly and low-level southwesterly winds, are closely related to an atmospheric heat source induced by differential heating between land and ocean (Kim and Wang 2011). Southwesterly winds prevail at 850 hPa during the East Asian summer monsoon, and northwesterly winds prevail in winter (Fig. 6a and b). Urbanization increased the summer wind in South China, but this wind decreased from 28°N to 40°N in East China (Fig. 6c). This may result in reduced northward water vapor transport. The combined effect of this reduction and decreased local available moisture is the main reason for the precipitation decline in northern city agglomerations. From Fig. 6d, we see that urbanization weakens winter wind in most of East China. This can diminish southward cold airflow, thereby strengthening urban warming to some degree.

Along longitude 115°E, upwelling movement is dominant in south of 35°N in summer (Fig. 7a). At low levels (below 600 hPa), airflow is southerly, opposite to that at high levels (above 300 hPa). After urbanization, updrafts near 26°N, 30°N, and 38°N are clearly invigorated (Fig. 7c). These locations basically correspond to the three urban agglomeration areas. Meanwhile, surrounding these areas, updrafts are weakened. Although upward motion is intensified by urbanization over the urban areas, no more precipitation is generated because of the lack of water vapor supply.

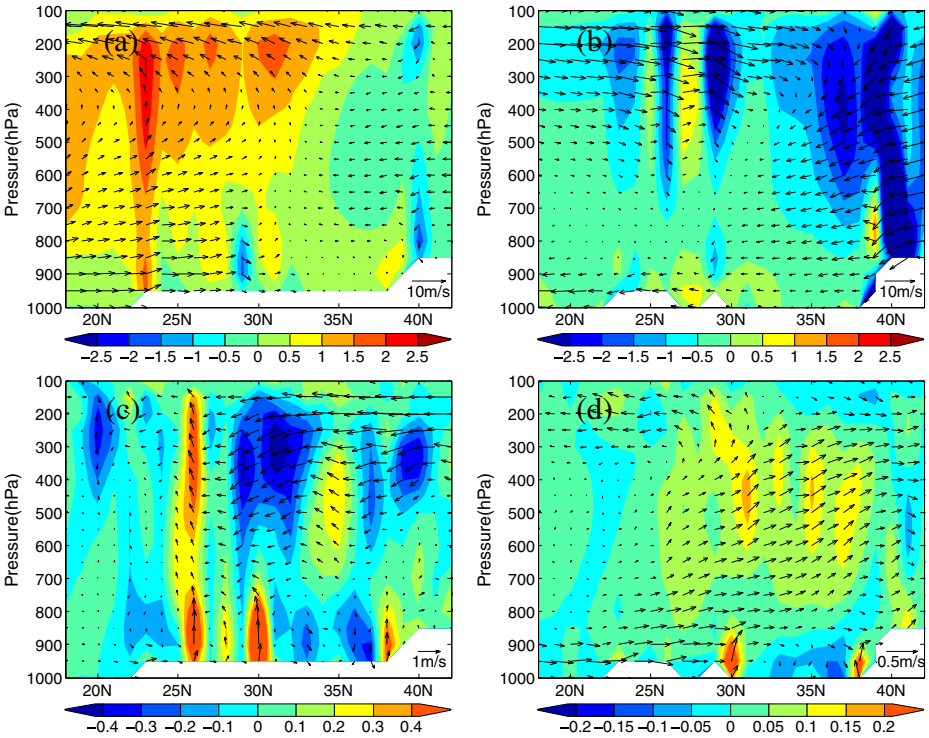

Fig. 7 Latitude-height cross section of control run in summer (**a**) and winter (**b**), plus its change caused by urbanization in summer (**c**) and winter (**d**). Shading represents vertical velocity at 115°E (Unit: cm/s)

In winter, downdrafts are dominant in most areas (Fig. 7b). There is only weak updraft below 900 hPa in most areas. After urbanization, downdrafts are weakened or updrafts strengthened in most areas, especially near 30°N and 38°N (Fig. 7d).

Although the urbanization mainly influences the climate and environment on local and regional scales, it is likely that large-scale urbanization will have a certain impact on the East Asian monsoon. To quantitatively investigate this impact, we analyze an East Asian monsoon index. Investigators have defined numerous indices for East Asian Summer Monsoon (EASM) strength, using circulation parameters instead of rainfall. This is due in part to complex rainfall structures and a preference toward using large-scale winds to define the broad-scale monsoon. In this study, according to present spatial patterns of East Asian monsoon configuration and limitations of the simulation domain, we used regionally averaged 850 hPa mean meridional wind speeds in winter and summer within 20°–40°N and 105°–125°E to measure large-scale intensity of the East Asian winter and summer monsoons (Wang 2002).

Figure 8 shows interannual variation of the East Asian summer and winter monsoon index during 2000–2009, including a comparison among the control run, NCEP-FNL and ERA-Interim, and change of monsoon index from urbanization. Because of forcing from the NCEP-FNL large-scale circulation, the model can better simulate the interannual variation of East Asian summer and winter monsoon index relative to NCEP-FNL and ERA-Interim. However, the simulated amplitude of index variation is larger than that observed (Fig. 8a and b). The correlation coeffecient of summer monsoon index between simulation and ERA-Interim is 0.80, and correlation of the winter index reached 0.91.

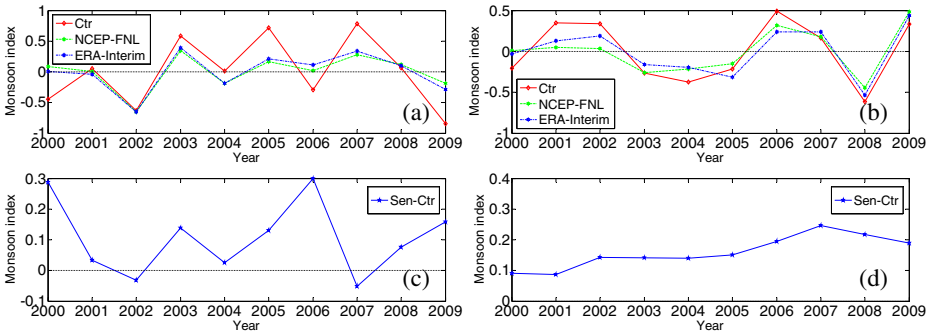

Fig. 8 Interannual variation of East Asian monsoon index of ERA-Interim, NCEP-FNL and control run in summer (**a**) and winter (**b**), plus its summer (**c**) and winter (**d**) change caused by urbanization during 2000–2009 (Unit: m/s)

The East Asian summer monsoon index increased after urbanization, except in 2002 and 2007 (Fig. 8c). The greatest changes were in 2006. From Fig. 6c, the summer wind decreased from 28°N to 40°N in East China. For calculating the monsoon index, we used meridional wind speeds at 850 hPa between 20°–40°N and 105°–125°E. In this region, there is a large area of increased summer wind to the east of 118°E. In winter, because the northerly wind prevails in East Asia, the positive value of monsoon index change causes a weakened winter monsoon. From Fig. 8d, because of urbanization, the East Asian winter monsoon is always weakened. The peak value appears in 2007.

Therefore, the intensity of East Asian Monsoon is mainly dominated by the large-scale circulation, but large-scale urbanization can likely affect it to some extent.

4 Discussion and conclusions

The climate effect of urbanization may be negligible on the global scale, but regional and local effects caused by urbanization cannot be neglected. In this paper, the long-term effect of urbanization on regional climate in China, especially on the East Asia monsoon, is investigated using the WRF model. On the basis of the previous study, the new gridded AHR data and the new parameterization of AHR are introduced to the WRF model to carry out the 10- year simulation, so the results can better illustrate the effects of urbanization on regional climate over China. In light of the calculation of inter-annual variability of urbanization effects, the magnitudes and ranges of urbanization effects are quantified, and more confident results are obtained.

By comparing with the observation, the WRF model has the capacity to simulate the interannual variation of regional climate in China.

After urbanization, surface albedo, surface available moisture, latent heat flux, and low cloud cover decrease. These factors all favor urban warming. The reduced low cloud cover does so by amplifying incident solar shortwave radiation at the surface. Over the urban agglomerations, the urbanization mainly results in the reduced precipitation from July to September, and precipitation change in August has a large interannual variability.

The urbanization weakens the 850 hPa summer wind from 28°N to 40°N in East China. The combined effect of decreased northward water vapor transport and decreased local available moisture is the main reason for precipitation reduction in the urban agglomerations.

Although upward motion is strengthened by urbanization, no more precipitation is produced because of the lack of water vapor supply.

Intensity of the East Asian monsoon is dominated by the large-scale circulation background, but large-scale urbanization will likely affect it to some degree. The East Asian summer monsoon index increased slightly with urbanization, but the winter monsoon was always weakened.

However, because of the complexity of the problem, uncertainties in parameterization of physical processes and forcing data in the model, uncertainties likely remain in the simulation results. The influence of aerosols on climate was not considered in the paper. Future work should estimate the effect of pollutant emissions on urban regional climate change. In view of physically-based sensitivity, ensemble simulations may be an efficient approach to reduce the uncertainties. In addition, the improvements of forcing data including AHR and physical process fitting for China are all-important factors for reducing the uncertainties.

Acknowledgements This study was supported by the Innovation Key Program of the Chinese Academy of Sciences (Grant No. KZCX2-EW-202), the National Key Program for Developing Basic Sciences of China (Grant No. 2009CB723904), the Special Scientific Research Fund of Meteorological Public Welfare Profession of China (Grant No. GYHY201106028), the General Project of the National Natural Science Foundation of China (Grant No. 41275108)

References

Allen L, Lindberg F, Grimmond C (2010) Global to city scale urban anthropogenic heat flux: Model and variability. International Journal of Climatology

Chen F, Kusaka H, Bornstein R et al (2010) The integrated WRF/urban modelling system: development, evaluation, and applications to urban environmental problems. International Journal of Climatology. doi:10.1002/joc.2158

Chen F, Dudhia J (2001) Coupling an advanced land-surface/hydrology model with the Penn State/NCAR MM5 modeling system. Part I: Model description and implementation. Mon Wea Rev 129:569–585

China Statistics Press (2009a) China City Statistics Yearbook. China Statistics Press, 488 pp.

China Statistics Press (2009b) China Energy Statistics Yearbook. China Statistics Press, 508 pp.

Dee DP, Uppala SM, Simmons AJ et al (2011) The ERA-Interim reanalysis: Configuration and performance of the data assimilation system. Q J Roy Meteor Soc 137(656):553–597. doi:10.1002/Qj.828

Emmanuel R, Krüger E (2012) Urban heat island and its impact on climate change resilience in a shrinking city: The case of Glasgow, UK. Building and Environment 53:137–149. doi:10.1016/j.buildenv.2012.01.020

Feng JM, Wang YL, Ma ZG, Liu YH (2012) Simulating the regional impacts of urbanization and anthropogenic heat release on climate across China. Journal of Climate 25(20):7187–7203. doi:10.1175/Jcli-D-11-00333.1

Flanner MG (2009) Integrating anthropogenic heat flux with global climate models. Geophysical Research Letters 36 (2). doi:10.1029/2008gl036465

Friedl MA, McIver DK, Hodges J, Zhang X, Muchoney D, Strahler A et al (2002) Global land cover mapping from MODIS: Algorithms and early results. Remote Sensing of Environment 83:287–302

Hamilton IG, Davies M, Steadman P et al (2009) The significance of the anthropogenic heat emissions of London's buildings: A comparison against captured shortwave solar radiation. Building and Environment 44(4):807–817. doi:10.1016/j.buildenv.2008.05.024

Huffman GJ, Adler RF, Bolvin DT, Gu G, Nelkin EJ, Bowman KP, Stocker EF, Wolff DB (2007) The TRMM multisatellite precipitation analysis (TMPA): Quasi-global, multiyear, combined-sensor precipitation estimates at fine scales. Journal of Hydrometeorology 8:38–55

IPCC (2007) Climate Change 2007: The Physical Science Basis. In: Solomon S, et al (eds) Contribution of Working Group I to the Fourth Assessment Report of the Intergovernmental Panel on Climate Change, Cambridge Univ. Press, Cambridge, U. K

Jiang X, Niu GY, Yang ZL (2009) Impacts of vegetation and groundwater dynamics on warm season precipitation over the Central United States. Journal of Geophysical Research 114 (D6). doi: 10.1029/2008jd010756

Jones PD, Lister DH, Li Q (2008) Urbanization effects in large-scale temperature records, with an emphasis on China. Journal of Geophysical Research 113 (D16). doi: 10.1029/2008jd009916

Kim H-J, Wang B (2011) Sensitivity of the WRF model simulation of the East Asian summer monsoon in 1993 to shortwave radiation schemes and ozone absorption. Asia-Pacific Journal of Atmospheric Sciences 47(2):167–180. doi:10.1007/s13143-011-0006-y

Lee SH, Song CK, Baik JJ, Park SU (2009) Estimation of anthropogenic heat emission in the Gyeong-In region of Korea. Theoretical and Applied Climatology 96(3):291–303

Lin CY, Chen WC, Chang PL, Sheng YF (2011) Impact of the urban heat island effect on precipitation over a complex geographic environment in Northern Taiwan. J Appl Meteorol Clim 50(2):339–353. doi:10.1175/2010jamc2504.1

Research Data Archive at the National Center for Atmospheric Research, Computational and Information Systems Laboratory, NCEP FNL Operational Model Global Tropospheric Analyses, continuing from July 1999.

Skamarock WC, Klemp JB, Dudhia J et al. (2008) A description of the advanced research WRF version 3. NCAR Tech. Note NCAR/TN-4751STR,125pp. [Available online at http://www.mmm.ucar.edu/wrf/users/docs/arw_v3.pdf.]

Shem W, Shepherd M (2009) On the impact of urbanization on summertime thunderstorms in Atlanta: Two numerical model case studies. Atmos Res 92(2):172–189. doi:10.1016/j.atmosres.2008.09.013

Wang HJ (2002) The instability of the East Asian summer monsoon-ENSO relations. Advances in Atmosphere Sciences 19(1):1–11

Wang J, Feng JM, Yan ZW, Hu YH, Jia GS (2012) Nested high-resolution modeling of the impact of urbanization on regional climate in three vast urban agglomerations in China. J Geophys Res-Atmos 117. doi: 10.1029/2012jd018226

Zhang CL, Chen F, Miao SG, Li QC, Xia XA, Xuan CY (2009) Impacts of urban expansion and future green planting on summer precipitation in the Beijing metropolitan area. J Geophys Res-Atmos 114. doi: 10.1029/2008jd010328

Zhang N, Gao Z, Wang X, Chen Y (2010) Modeling the impact of urbanization on the local and regional climate in Yangtze River Delta, China. Theoretical and Applied Climatology 102(3–4):331–342. doi:10.1007/s00704-010-0263-1

Zhang Y, Balzter H, Wu X (2013) Spatial–temporal patterns of urban anthropogenic heat discharge in Fuzhou, China, observed from sensible heat flux using Landsat TM/ETM+data. International Journal of Remote Sensing 34(4):1459–1477. doi:10.1080/01431161.2012.718465

Zhao TB, Fu CB (2006) Comparison of products from ERA-40, NCEP-2, and CRU with station data for summer precipitation over China. Adv Atmos Sci 23(4):593–604